

Model for the Thermodynamics of Iron at High Pressures Near Melting

Rann Shikler,^{*} Noya Dimanstein Firman, and Yinon Ashkenazy[†]
Racah Institute of Physics, Hebrew University of Jerusalem, Jerusalem 91904, Israel
(Dated: June 5, 2025)

The Fe pressure-temperature phase diagram and its melting line have a wide range of applications, including providing constraints for iron-core planetary models. We propose an equation of state (EOS) model based on the interstitial theory of simple condensed matter (ITCM) suggested by A.V. Granato [1]. When applied to Fe, this model allows for the extrapolation of measured melting lines to Earth's inner core boundary (ICB) conditions. The ITCM describes the solid-liquid phase transition in metals as resulting from a strong structural perturbation due to a high concentration of interstitial-like defects. The strong nonlinearity of their self-interaction causes the stabilization of this interstitial-rich phase. The original model is expanded to describe melting over a wide range of pressures and temperatures rather than focusing on a specific isobaric transition. Using this model, we fit the measured melting data, extrapolate it to cover ICB conditions, and develop a multiphase equation of state (EOS) that encompasses this regime. The model is used to explain contradictory data regarding the location of the melting line, resulting from a novel phase transition between two separate liquid phases, specifically between FCC-based and HCP-based liquids. This additional liquid phase offers a new interpretation of the previously suggested near-melting high-pressure phase [2] and may also provide a solution to the inner core nucleation paradox [3].

Introduction. — Iron's behavior at extreme pressures and temperatures is important in materials science and geophysics. Iron, the most abundant element in Earth's core, has a melting line and thermodynamic properties essential to understanding processes such as planetary formation, magnetic field generation, and seismic activity [4–10].

The melting temperature of iron under these conditions is evaluated using dynamic shock loading [11–14] and laser-heated diamond anvil cells (DAC) [15, 16]. While these techniques enable access to high temperatures and pressures, they yield significantly different results, with discrepancies of up to 3000 K in the estimated Fe melting temperature at Earth's inner core boundary (ICB) conditions [17]. These variations primarily arise from experimental limitations, such as limited access to combined high temperatures and pressures in DAC measurements and kinetic effects in shock wave experiments that may lead to observations of metastable states [18, 19]. The extrapolation of the melting line relies on fitting models to theoretical predictions, including density functional theory (DFT) calculations [20, 21] and multiphase equation of state calculations [7, 22, 23]. Thus models for the equation of state (EOS) of iron are needed both to extrapolate from experimental and theoretical specific evaluations as well as a platform to identify and explain contradictions between such values.

In this manuscript, we develop an EOS model to address these discrepancies and enhance our understanding of iron under ICB conditions. A significant limitation in developing such a model is the scarce availability of experimental data in the warm, dense regime. Our aim is to construct a thermodynamically consistent model for

Fe at the ICB conditions by extrapolating from available measurements of lower-temperature dense solid phases to higher temperatures. To that end we base our work on a class of models [1, 24–29] that describe the free energy difference between the solid and liquid phases by treating the liquid as a highly perturbed solid and estimation explicitly the variation of the free energy due to a specific microscopic perturbation. Consequently, these methods may allow for improved extrapolation of phase lines into regions that are not directly measured.

While a wide range of possible perturbations were considered in the past, many of these suffer from different contradictions, such as too high energy per atomic length energy to be generated thermally for dislocations [29] or too low entropy per volume in vacancy-based models[28].

We employed an EOS model based on Granato's interstitial theory of simple condensed matter (ITCM) [1, 30, 31]. This theory explains isobaric melting as a transition to a state with a high concentration of interstitial-like defects. The stabilization of the liquid, defect-rich phase is due to the strong nonlinearity of their self-interaction. Furthermore, Granato's model [1] was shown to be consistent with transport and kinetic processes. For example, solids with high interstitial concentrations simulated using Molecular Dynamics (MD) showed similar dynamics to those of liquids[32]. In addition, diffusion of interstitial-like defects was shown to control the crystallization velocity[33] with simulation being consistent with experiments at large supercooling [34].

Free Energy Model. — We extend the original model [1, 30, 31], which describes an isobaric phase transition, to a generalized form that covers a range of pressures and reconstructs the melting line over a broad thermodynamic regime.

Following Granato [1], we assume that the change in free energy caused by the addition of a single self-

^{*} rann.shikler@mail.huji.ac.il

[†] yinon.ash@mail.huji.ac.il

interstitial can be approximated by:

$$\Delta G = H_F - TS_F \quad (1)$$

Where H_F and S_F are the formation enthalpy and the formation entropy of interstitials, respectively.

The interstitial formation enthalpy is assumed to include two types of linear elastic contributions

$$\frac{dH_F}{dc} = (\alpha_1\mu(P, T, c) + \alpha_2B(P, T)) \cdot V(P, T, c) \quad (2)$$

where V , P and T are the volume, pressure and temperature, respectively, B and μ are the bulk and shear moduli and α_1 and α_2 are linear coefficients, it is assumed that $\alpha_1 \gg \alpha_2$. This is combined with a model, that most changes in the free energy due to strain are caused by changes in the formation enthalpy, which leads to the following expression for the shear modulus: $\mu(P, T, c) = \mu_0(P, T) \exp(-\alpha_1\beta c)$, Where β is a dimensionless free parameter that depends on the crystal structure, the resulting softening of the shear modulus with the interstitial concentration is consistent with experimental observations. [1]

The expression in Eq. 2 depends on the volume, for which we assume an exponential dependence on the interstitial concentration: $V(P, T, c) = V_0(P, T) \cdot e^{\xi c}$. Where ξ is a free parameter quantifying the relationship between interstitial concentration and volume change. This approximation was verified to produce a consistent expression with the volume obtained from the derivative of the free energy.

The entropy is assumed to include four major contributions [1, 30, 31]: frequency resonance modes, frequency local modes, frequency change due to volume change, and configuration entropy. Combined together, we get:

$$S_F = Nk_Bc \left[3\gamma\xi + \frac{4.35 \cdot \nu}{1 + a\alpha_1\beta c} - 4.25 + \ln \left(\frac{b}{\alpha_1\beta c} \right) \right] \quad (3)$$

Using Eq. 2, 3, the change in free energy of a crystalline system due to the addition of interstitials to a concentration of c can be written as:

$$\Delta G = \quad (4)$$

$$V_0 \left[\frac{\alpha_1\mu_0}{\xi - \alpha_1\beta} (e^{(\xi - \alpha_1\beta)c} - 1) + \frac{\alpha_2B}{\xi} (e^{\xi c} - 1) \right]$$

$$+ Nk_Bc \left[3\gamma\xi + \frac{4.35 \cdot \nu}{1 + a\alpha_1\beta c} - 4.25 + \ln \left(\frac{b}{\alpha_1\beta c} \right) \right]$$

This estimates the free energy of the perturbed crystalline state due to the addition of self-interstitials at a concentration of c .

It is assumed that the highly perturbed crystalline state is in fact the liquid state, and so $G_{Liquid} = G_{Solid} + \Delta G$. This approach is beneficial as it utilizes well-established EOS data and models for the solid phases, ensuring higher reliability.

Fitting. — The Helmholtz free energy for each solid phase is written as a combination of three terms:

$$F(\rho, T) = F_{cold}(\rho) + F_{ion}(\rho, T) + F_{electron}(\rho, T) \quad (5)$$

Where F_{cold} represents the T -independent "cold energy" and $F_{ion}, F_{electron}$, which represent changes to the free energy from ionic and electronic excitations, respectively. Treating ionic and electronic excitations as independent is a manifestation of the Born–Oppenheimer approximation, as is often assumed in EOS studies[22, 35–37].

To represent the cold term F_{cold} for each crystalline phase, we used the Vinet analytic form [22, 38]

$$F_{cold}(\rho) = E_0 + \frac{4B_0}{\rho_0(B'_0 - 1)^2} [1 - (1 + X) \exp(-X)] \quad (6)$$

in which $X = \frac{3}{2} (B'_0 - 1) [(\rho_0/\rho)^{1/3} - 1]$ where E_0, B_0 and B'_0 are the energy, bulk modulus, and the pressure derivative of the bulk modulus at the density of ρ_0 .

For the ionic-excitation term of the free energy F_{ion} , we used the Debye model [22, 39]

$$F_{ion}(\rho, T) = k_B T \left(\frac{9}{8} \frac{\theta(\rho)}{T} + 3 \ln \left\{ 1 - \exp \left[-\frac{\theta(\rho)}{T} \right] \right\} + D_3 \left[\frac{\theta(\rho)}{T} \right] \right) \quad (7)$$

where $\theta(\rho)$ is the Debye temperature fitted to a polynomial and D_3 is the third Debye function.

For the electronic-excitation term of the free energy $F_{electron}$, we used a model by Bushman[36]

$$F_{elc}(\rho, T) = C_V T \ln \left[1 + 0.5 \frac{\beta_e T}{C_V} \left(\frac{\rho_0}{\rho} \right)^{\gamma_e} \right] \quad (8)$$

where C_V, β_e and γ_e are the electronic heat capacity, electronic heat capacity coefficient and the electronic Grüneisen coefficient, respectively.

We fitted the free energies for the α (BCC), γ (FCC) and ε (HCP) phases to various experimental data. This includes: 1-bar T -dependent thermal-expansion [40, 41] and heat capacity (entropy) [42] data for the α and γ phases, Diamond Anvil Cell (DAC)[43] and principal Hugoniot measurements [44, 45], for α and ε phases, heated Hugoniot [46] for γ , ramp-compression data [47] for ε and the phase transition lines data [48, 49]. The fitted parameters are listed in [50]

To model the liquid state EOS, we use the fitted multiphase solid EOS and the change in free energy due to the high concentrations of interstitials in Eq. 4. Since the free energy of the liquid is described as a perturbed crystalline state, the fitting of the free energy was performed by identifying a solid state near melting and fitting a liquid phase transition using this phase as a reference. The properties of the underlying crystalline phase are predetermined by the fit within its thermodynamic stability range. This leaves as free-fitting parameters only

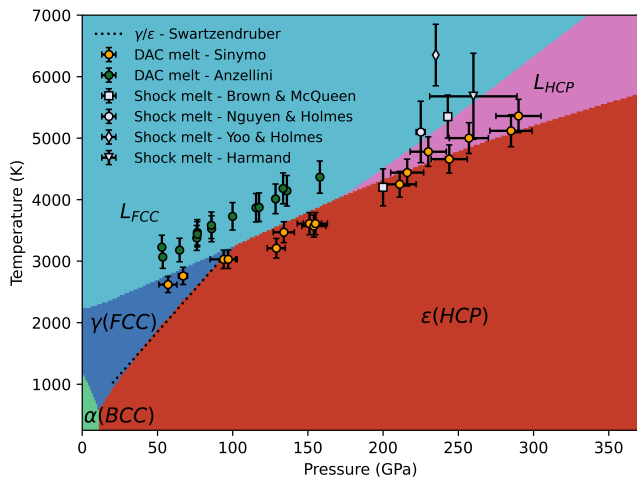


FIG. 1. Fe phase diagram derived from our multiphase EOS. Light green indicates the $\alpha(BCC)$ phase, blue indicates $\gamma(FCC)$, red indicates $\epsilon(HCP)$, light blue indicates L_{FCC} , pink indicates L_{HCP} . White markers indicate the Shock melt experiments where each marker indicates a different experiment: square[11], diamond[12], circle[13] and triangle[14]. The black dashed line indicates the $\gamma - \epsilon$ phase transition[49]. The orange[16] and green[15] circle indicates the DAC melt experiments.

those that describe interactions between the interstitials at high concentrations. We fitted liquid phases using only for γ (FCC) and ϵ (HCP) melting lines, which dominate at high pressures and have been previously fitted. The BCC-related α and δ phases are stable at lower pressures and are excluded due to their limited relevance. This fitting leads to two separate liquid free energies, namely, FCC- and HCP-based liquids, denoted as L_{FCC} and L_{HCP} .

The model was fitted to the melting line measurements from Sinmyo [16], as this dataset offers the broadest pressure range and closely approximates ICB conditions, enabling the most reliable extrapolation of the melting line. To maintain thermodynamic consistency, Richard's rule [51] was incorporated, governing the entropy change during melting. Additionally, bulk and shear moduli were independently fitted to a second-order pressure and first-order temperature expressions based on ab initio calculations [52–54], allowing for extrapolation beyond the regime where measurements of the solid phases are available.

Results and discussion. — A comparison between the phase diagram resulting from the fitted EOS to other calculations and measurements of the Fe melting line is presented in Fig. 1. The model was fitted to and reproduces melting data from DAC measurements by Sinymo[16] and disagrees with previous measurements by Anzellini [15]. Extrapolating the liquid phase free energies expression beyond their fitting range produced a hypothetical $L_{FCC} - L_{HCP}$ phase transition between the two liquid phases. The existence and location of this

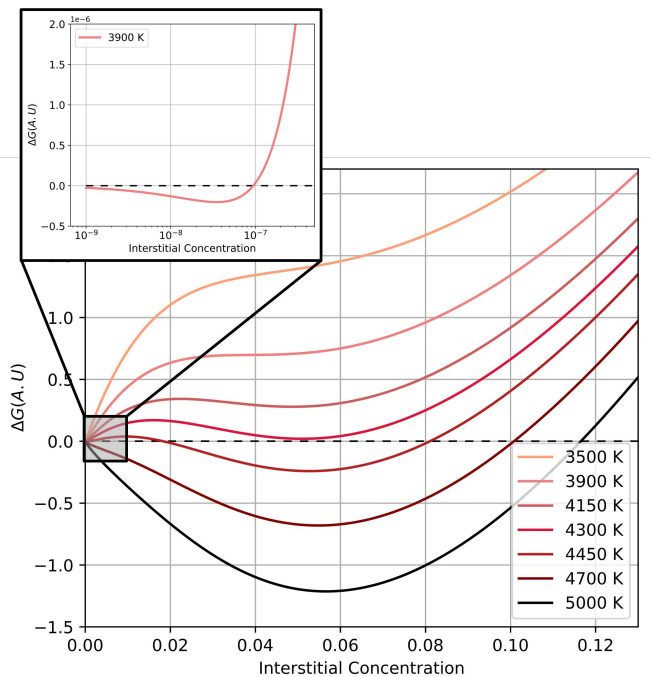


FIG. 2. The change in Gibbs free energy as a function of the interstitial concentration $\Delta G(c)$ at 200[GPa] at different temperatures near melting.

transition in the P-T phase diagram are not sensitive to a specific choice of fitting parameters. This phase transition agrees with results from shock melting experiments [11, 13, 14], and may explain the discrepancy between melting measurements at high pressure. Specifically, it reproduces the explicit observation of two-phase transitions measured by Brown & McQueen [11]. Such first-order liquid-liquid phase transitions were previously observed in experiments and atomistic simulations of other liquids, including liquid metals[55, 56].

The fitted EOS generates free energy curves that maintain the properties exhibited in the original isobaric transition model[1]. Specifically, it leads to a stable solid phase with a low concentration of $\sim 10^{-7}$ up to the melting temperature. And a stable high interstitial concentration phase with about 6% interstitial is expected to be amorphous and correspond to the liquid state, as illustrated in Fig. 2. At temperatures close to melting (within $\sim 10\%$ of T_M), local minima in the free energy at high and low c correspond to the existence of metastable liquid and solids. At temperatures outside this region, $T < 0.9T_M$ and $T > 1.1T_M$, $\Delta G_{s-l}(c)$ has only one minimum corresponding to the single stable phase.

In Fig. 3, the Hugoniot curves derived from the model are compared with shock melt measurements. The EOS leads to two closely spaced phase transition lines near melting at high pressures, one for melting and the other for the liquid-liquid phase transition. These two phase transitions are expected to lead to two separate transitions in the measured Hugoniot trajectory as it passes

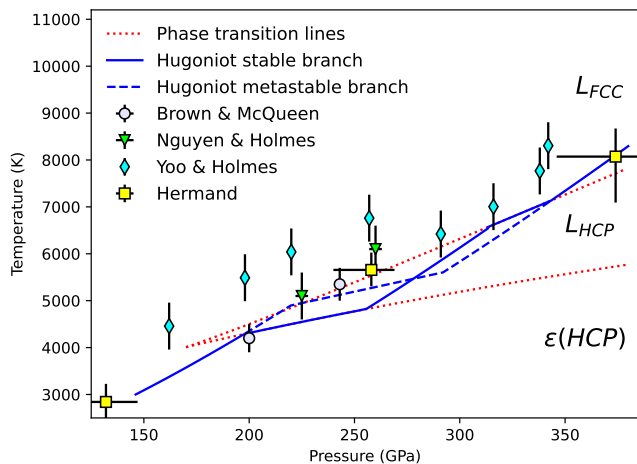


FIG. 3. The Hugoniot possible trajectories near melting. The red dotted lines indicate the $\varepsilon - L_{HCP}$ and the $L_{HCP} - L_{FCC}$ phase transitions. The solid blue line represents the derived Hugoniot trajectory, while the dashed blue line indicates a metastable branch that passes through the edges of the solid stability regime. The markers represent different shock melting measurements: gray circles[11], light blue diamonds[12], green triangles[13] and yellow squares[14].

through the transition zone. Such a double transition was reported in shock compression measurement of elastic velocities [11]. The theoretical Hugoniot curve passing through these phases is shown in Fig. 3, which agrees with measurements below and above the melting and the liquid-liquid phase transition lines. Between these lines, kinetics is expected to play a significant role as persistent metastable states are expected to be observed in dynamic experiments. The dashed line in Fig. 3 represents the Hugoniot trajectory continuing in metastable solid state until the upper limit of solid metastability. This leads to an improved fit to the measured data at 250(GPa)[11, 13, 14]. The optional trajectories corresponding to different transition points may explain the spread in the experimental data. Specifically, depending on kinetics, even a single transition from metastable solid to L_{FCC} , completely bypassing the intermediate liquid state, is possible. The measurements by Yoo and Holmes [12] deviate from our EOS, as shown in Figs. 1 and 3. This discrepancy may be attributed to the model used in [12] for the thermal capacity of the solid state, leading to differences in the estimated temperature, which is not directly measured.

In addition, seismic velocity measurements and simulations have shown that Earth’s inner core displays strong shear softening and an ultrahigh Poisson’s ratio. In simulations of Fe HCP solid close to melting, this softening was attributed to the formation of increased correlation in the displacement of atoms, manifested in chains of collective motion.[57] Such increased correlation in displacement chains was previously reported in atomistic simulations of Cu’s highly perturbed crystalline phase as

melting was approached.[32] Thus, this observed softening may be related to the suggested intermediate L_{HCP} . The formation of such an intermediate liquid phase is expected to reduce the nucleation barrier due to its effect on the solid-liquid interface energy[33, 34]. This, in turn, can explain the gap between the observed structure and the estimated nucleation time of the solid phase in Earth’s inner core. [3]. Furthermore, the L_{HCP} phase is a natural candidate as an intermediate phase for the two-step process, which was previously suggested to explain this phenomenon [58].

Another type of thermodynamic trajectories, that may be accessible experimentally, are the compression isotherms of the EOS presented in Fig. 4. The model’s entropy jump at melting is consistent with Richards’ rule [51], and the density profile follows a reasonable trend. [43]

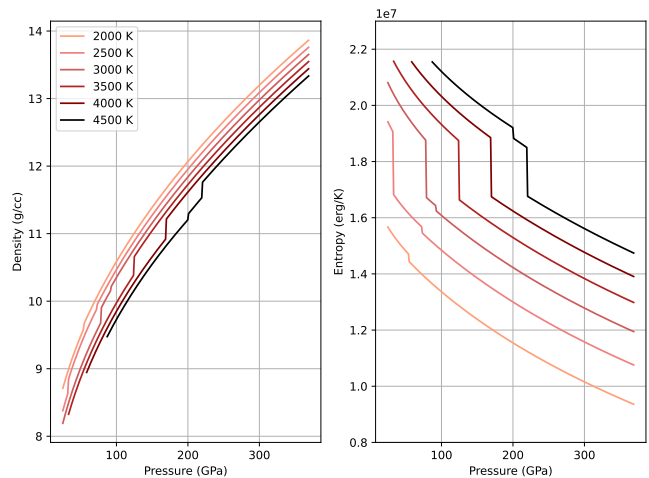


FIG. 4. Isotherms of (a) the density ρ and (b) the entropy S per gram at different temperatures. The vertical lines represent phase transitions along the isotherms, where the larger jumps indicate melting.

Conclusions. — Using ITCM, we derived expressions for the free energy functions of various iron phases at high pressure and temperature. Applying ITCM with two different solid reference phases at low temperatures leads to a phase diagram that includes two liquid phases. Calculations based on these functions coincide with measurements and prior computations.

The predicted $L_{HCP} - L_{FCC}$ phase transition line at high pressures is consistent with the divergence of existing melting measurements at high pressures. Furthermore, the L_{HCP} phase can explain the speculated high-pressure phase[2, 11].

ITCM’s liquid descriptions can have significant implications for Earth studies, such as predicting the melting lines for Fe under ICB conditions in a different method, explaining Earth’s inner core’s strong shear softening and an ultrahigh Poisson’s ratio, and a possible solution to the Earth’s inner core nucleation paradox.

This study represents the first application of ITCM with two reference states, achieving an improved fit to experimental data for iron under extreme conditions. The modified ITCM and derived free energy functions reveal

a potential liquid-liquid phase transition, consistent with observations and offering new insights into iron's behavior at high pressures.

-
- [1] A. V. Granato, Interstitialcy model for condensed matter states of face-centered-cubic metals, *Phys. Rev. Lett.* **68**, 974 (1992).
- [2] R. Boehler, The phase diagram of iron to 430 kbar, *Geophysical Research Letters* **13**, 1153 (1986).
- [3] L. Huguet, J. A. Van Orman, S. A. Hauck, and M. A. Willard, Earth's inner core nucleation paradox, *Earth and Planetary Science Letters* **487**, 9 (2018).
- [4] K. Hirose, S. Labrosse, and J. Hernlund, Composition and state of the core, *Annual Review of Earth and Planetary Sciences* **41**, 657 (2013).
- [5] F. D. Stacey, High pressure equations of state and planetary interiors, *Reports on Progress in Physics* **68**, 341 (2005).
- [6] Y. Kuwayama, G. Morard, Y. Nakajima, K. Hirose, A. Q. R. Baron, S. I. Kawaguchi, T. Tsuchiya, D. Ishikawa, N. Hirao, and Y. Ohishi, Equation of state of liquid iron under extreme conditions, *Phys. Rev. Lett.* **124**, 165701 (2020).
- [7] P. I. Dorogokupets, A. M. Dymshits, K. D. Litasov, and T. S. Sokolova, Thermodynamics and equations of state of iron to 350 gpa and 6000 k, *Scientific Reports* **7**, 41863 (2017).
- [8] Y. Zhang and J.-F. Lin, Molten iron in earth-like exoplanet cores, *Science* **375**, 146 (2022), <https://www.science.org/doi/pdf/10.1126/science.abn2051>.
- [9] J. Aubert, C. C. Finlay, and A. Fournier, Bottom-up control of geomagnetic secular variation by the earth's inner core, *Nature* **502**, 219 (2013).
- [10] M. Landeau, J. Aubert, and P. Olson, The signature of inner-core nucleation on the geodynamo, *Earth and Planetary Science Letters* **465**, 193 (2017).
- [11] J. M. Brown and R. G. McQueen, Phase transitions, grüneisen parameter, and elasticity for shocked iron between 77 gpa and 400 gpa, *Journal of Geophysical Research: Solid Earth* **91**, 7485 (1986).
- [12] C. S. Yoo, N. C. Holmes, M. Ross, D. J. Webb, and C. Pike, Shock temperatures and melting of iron at earth core conditions, *Phys. Rev. Lett.* **70**, 3931 (1993).
- [13] J. H. Nguyen and N. C. Holmes, Melting of iron at the physical conditions of the earth's core, *Nature* **427**, 339 (2004).
- [14] M. Harmand, A. Rivasio, S. Mazevet, J. Bouchet, A. Denoeud, F. Dorchies, Y. Feng, C. Fourment, E. Galtier, J. Gaudin, F. Guyot, R. Kodama, M. Koenig, H. J. Lee, K. Miyanishi, G. Morard, R. Musella, B. Nagler, M. Nakatsutsumi, N. Ozaki, V. Recoules, S. Toleikis, T. Vinci, U. Zastrau, D. Zhu, and A. Benuzzi-Mounaix, X-ray absorption spectroscopy of iron at multimegabar pressures in laser shock experiments, *Phys. Rev. B* **92**, 024108 (2015).
- [15] S. Anzellini, A. Dewaele, M. Mezouar, P. Loubeyre, and G. Morard, Melting of iron at earth's inner core boundary based on fast x-ray diffraction, *Science* **340**, 464 (2013).
- [16] R. Sinmyo, K. Hirose, and Y. Ohishi, Melting curve of iron to 290 gpa determined in a resistance-heated diamond-anvil cell, *Earth and Planetary Science Letters* **510**, 45 (2019).
- [17] R. Boehler, Temperatures in the earth's core from melting-point measurements of iron at high static pressures, *Nature* **363**, 534 (1993).
- [18] Y. Zel'dovich and Y. Raizer, *Physics of Shock Waves and High-Temperature Hydrodynamic Phenomena*, Dover Books on Physics (Dover Publications, 2012).
- [19] G. E. Duvall and R. A. Graham, Phase transitions under shock-wave loading, *Rev. Mod. Phys.* **49**, 523 (1977).
- [20] E. Sola and D. Alfè, Melting of iron under earth's core conditions from diffusion monte carlo free energy calculations, *Phys. Rev. Lett.* **103**, 078501 (2009).
- [21] D. Alfè, Temperature of the inner-core boundary of the earth: Melting of iron at high pressure from first-principles coexistence simulations, *Phys. Rev. B* **79**, 060101 (2009).
- [22] C. J. Wu, L. X. Benedict, P. C. Myint, S. Hamel, C. J. Prisbrey, and J. R. Leek, Wide-ranged multiphase equation of state for iron and model variations addressing uncertainties in high-pressure melting, *Phys. Rev. B* **108**, 014102 (2023).
- [23] S. K. Saxena and G. Eriksson, Thermodynamics of iron at extreme pressures and temperatures, *Journal of Physics and Chemistry of Solids* **84**, 70 (2015).
- [24] D. C. Wallace, Statistical mechanics of monatomic liquids, *Phys. Rev. E* **56**, 4179 (1997).
- [25] J. E. Lennard-Jones and A. F. Devonshire, Critical and co-operative phenomena. iii. a theory of melting and the structure of liquids, *Proceedings of the Royal Society of London. Series A. Mathematical and Physical Sciences* **169**, 317 (1939).
- [26] R. M. J. Cotterill, *Ordering in Strongly Fluctuating Condensed Matter Systems* (Plenum, New York, 1980).
- [27] H. Kleinert, *Gauge Fields in Condensed Matter* (WORLD SCIENTIFIC, 1989).
- [28] G. de With, Melting is well-known, but is it also well-understood?, *Chemical Reviews* **123**, 13713 (2023), pMID: 37963286, <https://doi.org/10.1021/acs.chemrev.3c00489>.
- [29] J. P. Poirier, Dislocation-mediated melting of iron and the temperature of the earth's core, *Geophysical Journal International* **85**, 315 (1986), <https://academic.oup.com/gji/article-pdf/85/2/315/2159261/85-2-315.pdf>.
- [30] A. Granato, Self-interstitials as basic structural units of liquids and glasses, *Journal of Physics and Chemistry of Solids* **55**, 931 (1994).
- [31] A. V. Granato, Interstitialcy theory of simple condensed matter, *The European Physical Journal B* **87**, 18 (2014).
- [32] K. Nordlund, Y. Ashkenazy, R. S. Averback, and A. V. Granato, Strings and interstitials in liquids, glasses and crystals, *Europhysics Letters* **71**, 625 (2005).
- [33] Y. Ashkenazy and R. S. Averback, Atomic mechanisms

- controlling crystallization behaviour in metals at deep undercoolings, *Europhysics Letters* **79**, 26005 (2007).
- [34] W.-L. Chan, R. S. Averback, D. G. Cahill, and Y. Ashkenazy, Solidification velocities in deeply undercooled silver, *Phys. Rev. Lett.* **102**, 095701 (2009).
- [35] D. Wallace, *Statistical Physics of Crystals and Liquids: A Guide to Highly Accurate Equations of State*, G - Reference, Information and Interdisciplinary Subjects Series (World Scientific, 2002).
- [36] A. Bushman, *Intense Dynamic Loading Of Condensed Matter* (Taylor & Francis, 1992).
- [37] A. V. Bushman and V. E. Fortov, Model equations of state, *Soviet Physics Uspekhi* **26**, 465 (1983).
- [38] P. Vinet, J. H. Rose, J. Ferrante, and J. R. Smith, Universal features of the equation of state of solids, *Journal of Physics: Condensed Matter* **1**, 1941 (1989).
- [39] P. Debye, Zur theorie der spezifischen wärmen, *Annalen der Physik* **344**, 789 (1912).
- [40] R. N. Abdullaev, R. A. Khairulin, and S. V. Stankus, Volumetric properties of iron in the solid and liquid states, *Journal of Physics: Conference Series* **1675**, 012087 (2020).
- [41] M. J. Assael, K. Kakosimos, R. M. Banish, J. Brillo, I. Egry, R. Brooks, P. N. Queded, K. C. Mills, A. Nagashima, Y. Sato, and W. A. Wakeham, Reference Data for the Density and Viscosity of Liquid Aluminum and Liquid Iron, *Journal of Physical and Chemical Reference Data* **35**, 285 (2006).
- [42] M. Chase, *NIST-JANAF Thermochemical Tables, 4th Edition* (American Institute of Physics, -1, 1998).
- [43] A. Dewaele, M. Torrent, P. Loubeyre, and M. Mezouar, Compression curves of transition metals in the mbar range: Experiments and projector augmented-wave calculations, *Phys. Rev. B* **78**, 104102 (2008).
- [44] L. M. Barker and R. E. Hollenbach, Shock wave study of the $\alpha \rightleftharpoons \varepsilon$ phase transition in iron, *Journal of Applied Physics* **45**, 4872 (1974).
- [45] J. M. Brown, J. N. Fritz, and R. S. Hixson, Hugoniot data for iron, *Journal of Applied Physics* **88**, 5496 (2000).
- [46] G. Q. Chen and T. J. Ahrens, High pressure and high temperature equation-of-state of gamma and liquid iron, *MRS Online Proceedings Library* **499**, 41 (1997).
- [47] R. F. Smith, D. E. Fratanduono, D. G. Braun, T. S. Duffy, J. K. Wicks, P. M. Celliers, S. J. Ali, A. Fernandez-Pañella, R. G. Kraus, D. C. Swift, G. W. Collins, and J. H. Eggert, Equation of state of iron under core conditions of large rocky exoplanets, *Nature Astronomy* **2**, 452 (2018).
- [48] J. C. Boettger and D. C. Wallace, Metastability and dynamics of the shock-induced phase transition in iron, *Phys. Rev. B* **55**, 2840 (1997).
- [49] L. J. Swartzendruber, The fe (iron) system, *Bulletin of Alloy Phase Diagrams* **3**, 161 (1982).
- [50] See Supplemental Material at [URL will be inserted by publisher], for the fitted parameters.
- [51] G. P. Tiwari, Modification of richard's rule and correlation between entropy of fusion and allotropic behaviour, *Metal Science* **12**, 317 (1978).
- [52] S. Ai, M. Long, S. Zhang, D. Chen, Z. Dong, P. Liu, Y. Zhang, and H. Duan, Ab initio calculations on elastic properties of if steel matrix phase at high temperature based on lattice expansion theory (2020).
- [53] R. E. Cohen, L. Stixrude, and E. Wasserman, Tight-binding computations of elastic anisotropy of fe, xe, and si under compression, *Phys. Rev. B* **56**, 8575 (1997).
- [54] P. Söderlind, J. A. Moriarty, and J. M. Wills, First-principles theory of iron up to earth-core pressures: Structural, vibrational, and elastic properties, *Phys. Rev. B* **53**, 14063 (1996).
- [55] P. McMillan, Jumping between liquid states, *Nature* **403**, 151 (2000).
- [56] G. Franzese, G. Malescio, A. Skibinsky, S. V. Buldyrev, and H. E. Stanley, Generic mechanism for generating a liquid-liquid phase transition, *Nature* **409**, 692 (2001).
- [57] Y. Zhang, Y. Wang, Y. Huang, J. Wang, Z. Liang, L. Hao, Z. Gao, J. Li, Q. Wu, H. Zhang, Y. Liu, J. Sun, and J.-F. Lin, Collective motion in hcp-fe at earth's inner core conditions, *Proceedings of the National Academy of Sciences* **120**, e2309952120 (2023), <https://www.pnas.org/doi/pdf/10.1073/pnas.2309952120>.
- [58] Y. Sun, F. Zhang, M. Mendeleev, R. Wentzcovitch, and K. M. Ho, Two-step nucleation of the Earth's inner core, in *AGU Fall Meeting Abstracts*, Vol. 2021 (2021) pp. DI35D-0058.

Supplemental Materials: Model for the Thermodynamics of Iron at High Pressures Near Melting

Rann Shikler,* Noya Dimanstein Firman, and Yinon Ashkenazy†
Racah Institute of Physics, Hebrew University of Jerusalem, Jerusalem 91904, Israel
 (Dated: June 5, 2025)

In this Supplemental Material, we supply the model-fitted parameters required to recreate results described in this manuscript.

I. SOLID FITTING

The parameters listed below correspond to the fitted equations of state and thermodynamic properties of solid iron phases ($\gamma(FCC)$ and $\varepsilon(HCP)$). These parameters were obtained by fitting the Helmholtz free energy formulation described in the main text [5–8].

TABLE I. Solid fitting parameters

Phase	$E_0[\text{erg}]$	$B_0[\text{GPa}]$	B'	$\rho_0[\frac{\text{g}}{\text{cc}}]$	$C_v[\frac{\text{erg}}{\text{K}}]$	$\beta_e \cdot \rho_0^{\gamma_e}$	γ_e
$\gamma(FCC)$	$8.37 \cdot 10^8$	130.6	7.34	8.226	$1.4 \cdot 10^6$	$1.7 \cdot 10^7$	2.86
$\varepsilon(HCP)$	$8.8 \cdot 10^8$	182.9	5.56	8.445	$1.64 \cdot 10^6$	$1.1 \cdot 10^7$	3.33

The Debye temperature $\theta(\rho)$ described in [7] was fitted using a fourth-order polynomial, as shown in Table II.

TABLE II. Debye temperature $\theta(\rho) = \sum_0^n c_i \rho^i$

Phase	c_0	c_1	c_2	c_3	c_4
$\gamma(FCC)$	-41.739	141.568	-23.36	1.863	-0.0365
$\varepsilon(HCP)$	-39.845	147.571	-25.602	1.805	-0.0307

II. LIQUID FITTING PARAMETERS

The liquid phase thermodynamic parameters were fitted to the model described in the main text [4]. Table III lists the optimized parameters for both FCC-like and HCP-like liquid states.

TABLE III. Liquid fitting parameters

Phase	β	α_1	α_2	a	b	ν	ξ
L_{FCC}	55	1.1	0.035	0.041	0.1	4	0.28
L_{HCP}	55	0.97	0.0005	0.37	0.14	10	0.07

* rann.shikler@mail.huji.ac.il

† yinon.ash@mail.huji.ac.il